Laser-driven shock experiments on precompressed water: Implications for "icy" giant planets

Kanani K. M. Lee[a)]
Department of Earth & Planetary Science, University of California–Berkeley, Berkeley, California 94720-4767 and Department of Physics, New Mexico State University, MSC 3D, Las Cruces, New Mexico 88003-8001

L. Robin Benedetti
Physics Department, University of California–Berkeley, Berkeley, California 94720-7300 and Lawrence Livermore National Laboratory, Livermore, California 94550

Raymond Jeanloz
Department of Earth & Planetary Science, University of California–Berkeley, Berkeley, California 94720-4767

Peter M. Celliers, Jon H. Eggert, Damien G. Hicks, Stephen J. Moon, Andrew Mackinnon, Luis B. Da Silva, David K. Bradley, Walter Unites, and Gilbert W. Collins
Lawrence Livermore National Laboratory, Livermore, California 94550

Emeric Henry, Michel Koenig, and Alessandra Benuzzi-Mounaix
Laboratoire LULI, Ecole Polytechnique, 91128 Palaiseau, France

John Pasley
Center for Energy Research, University of California at San Diego, San Diego, California 92093-0417

David Neely
Central Laser Facility, Rutherford Appleton Laboratory, Oxfordshire OX11 0QX, United Kingdom

(Received 11 November 2005; accepted 2 May 2006; published online 5 July 2006; publisher error corrected 29 November 2006)

Laser-driven shock compression of samples precompressed to 1 GPa produces high-pressure-temperature conditions inducing two significant changes in the optical properties of water: the onset of opacity followed by enhanced reflectivity in the initially transparent water. The onset of reflectivity at infrared wavelengths can be interpreted as a semiconductor↔electronic conductor transition in water, and is found at pressures above ~130 GPa for single-shocked samples precompressed to 1 GPa. Our results indicate that conductivity in the deep interior of "icy" giant planets is greater than realized previously because of an additional contribution from electrons.
© *2006 American Institute of Physics*. [DOI: 10.1063/1.2207618]

I. INTRODUCTION

Although giant gas planets such as Jupiter and Saturn are mostly comprised of hydrogen and helium, others such as Neptune and Uranus are additionally believed to contain as much as ~50% water (by mass) and significant amounts of methane and ammonia.[1] In the astronomical literature, these compounds are labeled "ices" regardless of physical state, in order to distinguish them from hydrogen, helium, or the heavier elements ("metals") and to emphasize their molecular character at low pressures and temperatures. In fact, most of the water in Neptune and Uranus is expected to be present as a dense fluid layer (possibly in a dissociated state) at pressures ranging between 20 and 600 GPa and temperatures between 2500 and 7000 K (Fig. 1), and it is hypothesized that it is in this "icy" layer that the planet's magnetic field is produced.[1]

Planetary magnetic fields are prevalent in our Solar System, are expected to be common among extrasolar planets, and can reveal important information about the interiors and evolutionary histories of planets.[2] Three potential mechanisms can generate planetary magnetic fields: permanent magnetism, which is produced at the microscopic level and is inherent to the material (e.g., ferromagnetism), induction from external sources, or production through electrical currents generated by a dynamo. Although some of the magnetism in our Solar System can be attributed to permanent magnetism from iron-rich minerals (e.g., Moon and Mars) or by induction by varying external magnetic fields (Galilean satellites), most must be formed by a dynamo sustained by convection of an electrically conducting fluid deep inside the planet. Together with moment of inertia measurements, magnetic field observations offer some of the most direct information about the constitution and processes of planetary interiors.

The magnetic fields of Neptune and Uranus were first measured during the Voyager 2 mission.[3] The surface field was shown to be about the same for both planets, $\sim 2 \times 10^{-5}$ T, comparable in strength to the Earth's magnetic

[a)]Author to whom correspondence should be addressed. Electronic mail: kanani@physics.nmsu.edu

 © 2006 American Institute of Physics

Downloaded 01 Feb 2008 to 128.115.27.10. Redistribution subject to AIP license or copyright; see http://jcp.aip.org/jcp/copyright.jsp

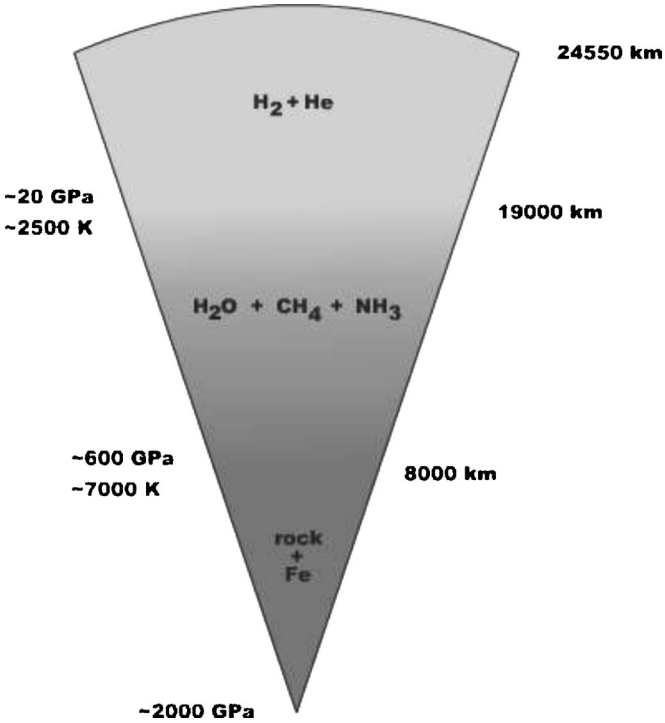

FIG. 1. Interior model of "icy" giant planets Uranus and Neptune, showing the approximate chemical makeup as a function of depth (Ref. 1). Left-hand side yields model pressure and temperature for the H–He envelope, "icy" mantle layer, and rocky core for Neptune. The right-hand side shows the corresponding radii for each layer. It is expected that it is in the icy mantle that the strong quadrupolar magnetic field is produced.

field value of $\sim 5\times 10^{-5}$ T. Although it is expected that the "icy" giant planets have a core of "ice," rock, and metal about the size of the Earth, the mostly quadrupolar nature of their observed magnetic fields suggests that an Earth-type iron-dominated geodynamo near the center of the planet is unlikely to be the source of the magnetism. The large radius of an icy giant planet dictates that for such a strong quadrupole field to be observed, with its strength falling as r^{-4} where r is radial distance, the source must be at shallower depths. It is thus thought that an ionic or perhaps metallic form of water, existing at the high pressures (20–600 GPa) and temperatures (2500–7000 K) in the shallower depths ($\sim$6000–17 000 km deep) of the planet, sustains the necessary electric currents for the planetary dynamo (Fig. 1).[1]

An electrical conductivity of at least $\sim 10\ (\Omega\ \mathrm{cm})^{-1}$ is thought to be required to generate the observed magnetic fields.[4] Conductivity values of up to $\sim 10-\sim 200\ (\Omega\ \mathrm{cm})^{-1}$ have been measured for both shock-compressed water[5–7] and for a "synthetic Uranus"[8] mixture of fluids, and have been predicted by molecular dynamics simulations.[9] A larger value of conductivity relaxes the velocity and length scales for a self-sustaining dynamo.[2] For instance, the magnetic Reynolds number, Re, is proportional to the product of the conductivity, length, and velocity scales. With a Re value of 10 or more a dynamo is self-sustaining,[2] and if the conductivity value is increased the length and velocity scales can be decreased for a given Re. This is of interest because a recent dynamo model suggests that in order to match the magnetic field morphology for a planet such as Neptune or Uranus, the dynamo is formed by a thin, conducting fluid shell above a stably stratified, conducting fluid interior and small solid core.[10]

High-pressure and high-temperature conditions have been simulated in the laboratory with diamond-anvil cells (DACs) and through shock-wave experiments. Successful DAC experiments have been carried out on water to 210 GPa at temperatures near 300 K (Refs. 11 and 12) and at lower pressures but higher temperatures,[13–19] leaving much of the pressure range relevant to the icy layer uninvestigated (Fig. 1). Shock compression produces high pressures and temperatures during the time that the shock wave is passing through the sample. The time scales are short ($\sim 10^{-10}-10^{-6}$ s), but longer than the time required for thermal equilibrium ($\sim 10^{-14}-10^{-11}$ s). Early Soviet shock-wave experiments, produced by nuclear explosions, reached up to 3200 GPa in water.[20,21] More recently, laser-driven shock experiments on water have reached pressures up to nearly 800 GPa with estimated temperatures greater than 30 000 K.[22] Reverberating-shock experiments on water have reached 180 GPa (Ref. 7) and $\sim$5400 K (temperatures reevaluated in a separate study[22,23]). Previous single-shock gas gun experiments were limited to pressures below 100 GPa.[6,24–26]

Static compression typically yields an equation of state (EOS) along an isotherm, and at pressures above 100 GPa, static methods are often difficult to implement at temperatures greater than $\sim$3000 K. Single-shock methods probe the EOS along a well-defined pressure-temperature (P-T) path (Hugoniot) yielding quantitative measures of density (ρ) and internal energy (E), however, only intersect a planet's isentrope at one point. By combining the two methods, laser-driven shock experiments on precompressed samples access conditions unreachable by either static or single-shock techniques alone, covering a broad range of P-ρ-T space and increasing access to the isentrope.[27,28]

Knowing the initial pressure and density of the precompressed sample, it is possible to infer the P-ρ-E conditions achieved in the sample under shock compression via the Rankine-Hugoniot relations,[29]

$$\rho_0 U_S = \rho_1 (U_S - u_p), \tag{1}$$

$$P_1 - P_0 = \rho_0 U_S u_p, \tag{2}$$

$$E_1 - E_0 = \frac{1}{2}(P_0 + P_1)\left(\frac{1}{\rho_0} - \frac{1}{\rho_1}\right), \tag{3}$$

where ρ is density, U_S is shock velocity, u_p is particle velocity, P is pressure, E is internal energy, and subscripts 0 and 1 are the initial and final states. Equations (1)–(3) describe the conservation of mass, linear momentum, and energy.

Here we present EOS and optical measurements using laser-driven shock waves on precompressed samples of water. The EOS measurements are expected to lie between the principal isentrope and principal Hugoniot of water, due to the increased initial density of the precompressed sample, thereby approaching conditions close to those of the icy layers of Neptune and Uranus. We also observe optical changes in the shock-compressed water under planetary-interior con-

Downloaded 01 Feb 2008 to 128.115.27.10. Redistribution subject to AIP license or copyright; see http://jcp.aip.org/jcp/copyright.jsp

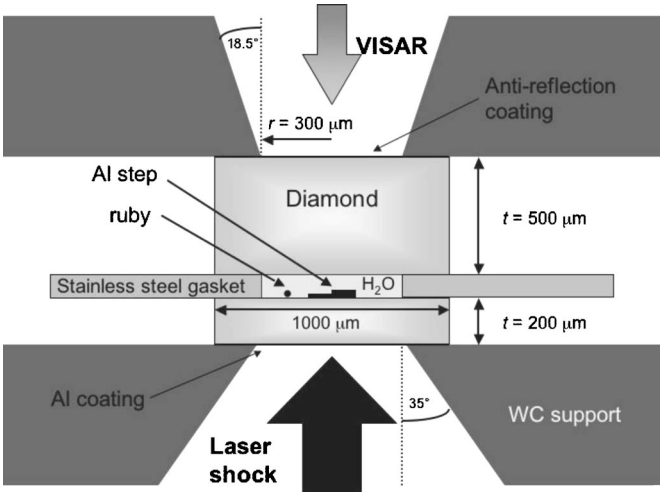

FIG. 2. Schematic cross section of diamond-cell configuration used for laser-driven shock experiments on precompressed samples. Wide openings (300 μm radius holes) in tungsten carbide (WC) supports allow ample shock-laser entry (35° opening) and VISAR access (18.5° opening). Thin diamonds are pushed together to apply pressure on a small sample of water (~30 nl), held in a hole within a stainless steel gasket 100 μm thick. A stepped Al foil is glued on the thinnest diamond and used to measure U_S(Al) with VISAR. A few ruby spheres are placed in the sample chamber for precompression pressure measurements via ruby fluorescence (Ref. 45). There is a 1000 Å Al flash coating on the laser-shock side of the thinnest diamond, in order to lower the critical depth of shock ablation, and an antireflection coating on the thicker diamond for the VISAR measurement.

ditions, and these provide evidence for a change in the electrical conduction mechanism in H_2O relevant for understanding the production of magnetic fields in the icy giant planets.[9,22]

II. METHODS

The sample consists of a layer of pure (doubly distilled) water compressed between two diamond windows, with an aluminum foil embedded in the water layer and placed against the diamond window from which the shock wave enters (Fig. 2). The aluminum foil is used for calibration of the shock-wave velocity: it is stepped, such that the shock wave traverses two distinct thicknesses before entering the water.[22,27,28] Modified DACs fit with 200–500 μm thick, 1.0 mm in diameter diamond windows, were used to compress water to a finite initial density and pressure (see Table I), and were shocked by a high-power laser pulse (Table II).[30] A detailed description of the design of the precompressed targets has been given elsewhere.[27] These experiments were performed at the Vulcan Laser Facility at the Rutherford Appleton Laboratory.[30] Shots identified with a "00" prefix were driven with a 4 ns square laser pulse composed of a series of stacked 1 ns pulses, whereas a "01" prefix identifies experiments driven with a 1 ns square pulse. The longer-duration pulses yield a more steady shock throughout the sample; the short pulses have increased power density, so provide stronger shocks.

For each shot, there were three probes monitoring the sample: two velocity interferometer system for any reflector (VISAR) interferometers (Figs. 3 and 4) and an optical pyrometer.[28,31–33] For all 00 shots, both interferometers were operated at 532 nm, whereas all 01 shots were recorded by an interferometer operating at 532 nm and a second operating at 1064 nm. A streaked optical pyrometer was also used to measure the blackbody radiation emitted from the shocked sample. The absolute calibration on the pyrometric measurement was not accurate enough to determine temperatures to better than ~35% uncertainty at the highest pressures. For this reason, we calculate the temperatures of the shocked precompressed water using the model of Ree,[34] available in the SESAME database,[35] T_{SESAME} (Table II). This equation-of-state model matches the measured principal Hugoniot of water to over 800 GPa,[22] and we use it to estimate the shock temperatures for water off the principal Hugoniot.

III. ANALYSIS

The analysis of the VISAR records reveals changes in the optical properties of water from its initially transparent state: with increasing shock pressures and temperatures, water becomes optically opaque ($T_{\mathrm{SESAME}} > \sim 3000$ K) and then reflecting ($T_{\mathrm{SESAME}} > \sim 6000$ K). Because VISAR requires a reflecting surface, the changing optical properties of

TABLE I. Experimental conditions for precompressed samples. Initial pressures P_0 are measured by ruby fluorescence (Ref. 45), while initial water densities ρ_0 are calculated from P_0 (Ref. 46). Diamond thicknesses and Al step heights are known to better than 2%. Uncertainties are listed below each measured value in parentheses.

Sample	P_0 (GPa)	ρ_0 (g/cm^3)	Drive diamond thickness (μm)	VISAR diamond thickness (μm)	Al step heights 1, 2 (μm)	Al step diameter (μm)	Initial gasket thickness (μm)
001212-13	0.75	1.199	200	500	6.3	200	100
	(0.07)	(0.005)			11.5		
001213-12	0.93	1.229	200	500	0.12	200	100
	(0.13)	(0.018)			16.6		
001222-6	0.68	1.195	200	500	11.9	200	100
	(0.07)	(0.008)			16.3		
011218-07	1.02	1.242	200	500	5.4	400	100
	(0.02)	(0.002)			15.3		
011220-06	0.40	1.127	200	500	5.7	400	100
	(0.005)	(0.001)			15.7		

Downloaded 01 Feb 2008 to 128.115.27.10. Redistribution subject to AIP license or copyright; see http://jcp.aip.org/jcp/copyright.jsp

TABLE II. Final-state values (determined at the shock breakout from the Al) of our shocked precompressed water samples. The shock velocities for Al are measured by VISAR. Particle and shock velocities for water, $u_p(H_2O)$ and $U_S(H_2O)$, are determined by the fringe shift in the short step of the Al, where attenuation is less, for transparent (reflecting) water. For opaque and reflecting shots, $u_p(H_2O)$ is determined by impedance match with the Al step (Refs. 34, 35, and 37). Italicized values are calculated from the SESAME database (Ref. 35) Table 7150 (Ref. 34). The final pressures and densities are calculated through the Rankine-Hugoniot relations (Ref. 29). Optical properties are given in the first column. Temperature estimates from the SESAME database (Ref. 35), Table 7150 (Ref. 34), are given in the final column. Uncertainties are listed below each measured value in parentheses.

Sample	U_S(Al) (μm/ns)	$U_S(H_2O)$ (μm/ns)	$u_p(H_2O)$ (μm/ns)	$P_f(H_2O)$ (GPa)	$\rho_f(H_2O)$ (g/cm^3)	T_{SESAME} (K)
4 ns laser-shock pulse, VISAR interferometry at 532 nm only						
001212-13 transparent	10.3 (0.3)	8.7 (0.2)	4.5 (0.2)	47 (4)	2.47 (0.15)	2 100 (200)
001213-12 opaque	13.0 (0.4)	12.3 (0.3)	7.4 (0.3)	112 (8)	3.08 (0.20)	5 500 (600)
001222-6 reflecting (532)	17.3 (0.4)	17.6 (0.4)	12 (0.4)	250 (15)	3.75 (0.20)	19 000 (1 700)
1 ns laser-shock pulse, VISAR interferometry at 532 and 1064 nm						
011218-07 reflecting (1064)	15.5 (0.7)	14.9 (0.4)	10.0 (0.8)	185 (20)	3.77 (0.35)	10 800 (1 700)
011220-06 reflecting (1064) opaque (532)	15.1 (0.4)	15.3 (0.3)	9.8 (0.4)	169 (10)	3.14 (0.25)	12 500 (1 200)

the sample must be considered and are described below for each optical character observed. Reflectivity is estimated by determining the intensity of light measured after the shock breaks out from the Al step (reflectivity of ~80% in a spectral range of 550–580 nm).[36] In samples that remain transparent ($T_{SESAME} < \sim 3000$ K), the intensity of the light after breakout is within 5% of that reflected from unshocked Al; that is, the water continues to stay transparent to the light being reflected off the moving Al step (Fig. 3). For opaque samples (~ 3000 K $< T_{SESAME} < \sim 6000$ K), the intensity of light after breakout from the Al step drops to less than 5% of that reflected from unshocked Al. We estimate that the absorption of light takes place, within an optical depth of less than 1 μm. Samples identified as reflecting were observed to reflect the probe light from the shock front, rather than from the moving Al-water interface, and are identified as such with Al-shock velocities that are greater than those that have been identified as opaque (Fig. 4, Table II). Uncertainties in the absolute value of the reflectivity are significant (up to 20%–40%) owing to imperfections in the Al surface and the antireflection coatings we use, as well as the presence of ice VI crystal formation for the highest precompression pressures. However, the onset of reflectivity was clearly observed at a detection limit of ~3%–5%. Initial conditions, measured and calculated velocities, and final conditions as determined by the Rankine-Hugoniot relations and impedance matching[29] are listed in Tables I and II.

IV. RESULTS

We determine the shock velocity of Al, U_S(Al), from the difference between the breakout times in the low and high steps of the Al foil, the thicknesses of which were measured by white-light interferometry before and after precompression. We find that the thickness of the step height does not change appreciably during precompression, due to the low pressures applied and the relatively high bulk modulus of Al. We calculate the particle velocity of the Al, u_p(Al), through empirical linear U_S-u_p relations.[37] For transparent samples, it is also possible to measure the particle velocity in the water, $u_p(H_2O)$, by the VISAR data.[31,33,38,39] Uncertainties in the U_S(Al) determination are reduced due to the redundant interferometers, but can be as large as 5%. To determine the conditions reached in the shocked precompressed water, we use impedance matching techniques[29] and the SESAME tables.[34,35]

Water is transparent at ambient conditions, and continues to be so along the principal Hugoniot until ~30 GPa.[26,40] In one of our shots, we find that water remains transparent at pressures exceeding 100 GPa at temperatures less than 3000 K. In this shot, 001212-13 (Fig. 3), we observe a leading shock as it is overtaken by a second, stronger shock. The first discontinuity in the VISAR image is the first shock wave as it breaks through the Al step into the precompressed water: the water remains transparent and the observed reflection originates from the Al-water interface. The next discontinuity indicates the arrival of the second shock at the Al-water interface, and the final discontinuity indicates the second shock overtaking the first shock, producing conditions that make the water opaque. Calculations designed to match the observed interface velocities indicate that the two shocks compressed the sample to two distinctive *P*-*T* conditions at which the water continues to be transparent: ~47 GPa and 2100 K, and ~125 GPa and 2800 K.

At pressures above ~50 GPa along the single-shock Hugoniot of normal water, previous studies have shown wa-

Downloaded 01 Feb 2008 to 128.115.27.10. Redistribution subject to AIP license or copyright; see http://jcp.aip.org/jcp/copyright.jsp

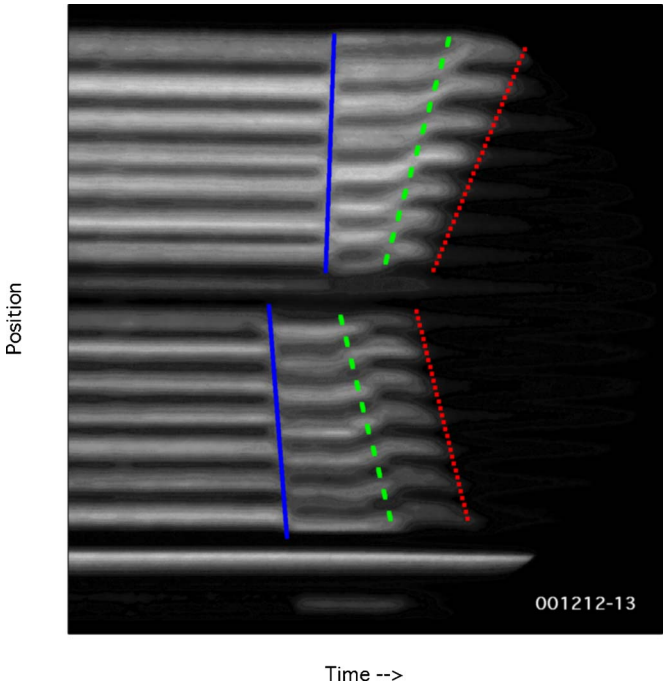

FIG. 3. VISAR streaked image at 532 nm for sample 001212-13. The time duration for this shock record is ~5 ns and the vertical axis is ~200 μm. Al step breakouts are outlined in blue for the high and low steps. The water is transparent and continues to be so after another shock enters the sample (green dashed line). A final shock enters the sample, finally making the water opaque (red dotted outline).

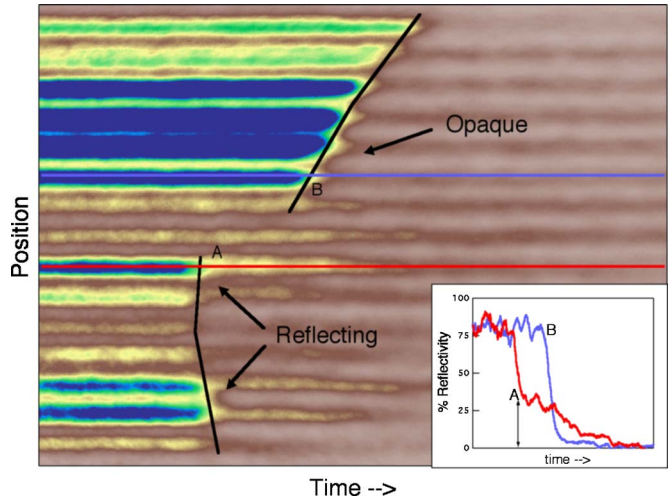

FIG. 4. VISAR streaked image at 1064 nm for sample 011218-07. Al step breakouts are shown for the short (A) and tall (B) steps. The time duration for the shock record shown is ~5 ns and the vertical axis is ~400 μm. This sample was precompressed to the ice VI[47] structure of water before undergoing shock conditions. Note that the intensity of light reflected after the short aluminum step (A) is still high, although not visible for the tall step (B). This is likely due to the decreased shock strength after going through ~10 μm of additional Al. Measured pressure and calculated temperature at (A) is ~185 GPa and 10 800 K. Variations in the reflected-light intensity along the spatial dimension is likely due to scattering of light from ice VI crystals that grew in the precompressed water. Inset: percent reflectivity as a function of time. In red (blue), a normalized lineout of the intensity used as a proxy for reflectivity, for the short (tall) step. There is a decaying intensity reflected off the short Al step, corresponding to ~30% reflectivity compared to ~80% reflectivity for the Al step.

ter to be opaque.[24] We also observe water to be opaque at high pressures and temperatures. The opacity of the water is confirmed by a low reflectivity and the lack of fringe shift after the Al-shock breakout in both VISAR records (low intensity fringes remain as a result of ghost reflections from the external surface of the diamond window).

An example of a reflecting VISAR record is shown in Fig. 4. The first two fringe discontinuities are due to the Doppler shift of the moving Al-water interface. Since the reflected light originates from the shock front, the fringe shift yields the shock velocity in the water, U_S(water). As the water is precompressed, the pressure-dependent index of refraction of water ($n=1.37-1.45$ at our initial compressions of 0.40–1.02 GPa, as opposed to 1.33 at ambient pressure)[41] was taken into account in determining the shock velocities.[33] We also observe the intensity of reflected light decrease as the shock wave decays in amplitude, with the water becoming opaque in the infrared at ~130 GPa along the precompressed 1 GPa Hugoniot of water (Figs. 4 and 5). This is similar to previous observations along the principal Hugoniot, showing the onset of reflectivity near ~100 GPa.[22] Combining these observations, the transition from opaque to reflecting behavior is found to be pressure and temperature dependent with a transition slope of approximately −12 K/GPa, although the uncertainties could be as much as ±9 K/GPa.

V. DISCUSSION

In a previous work[22] we modeled the reflectivity using a semiconductor formalism to estimate the free carrier density with a Drude model to calculate the electronic conductivity σ_e. In this model, we empirically fit reflectivity data at 532 and 1064 nm along the principal Hugoniot and calculated the free carrier density and σ_e. A linear temperature and density dependence of the gap energy was included in the fit.[22] We find that this model is consistent with our current observations of shocked precompressed water, and it is used in our current analyses.

In Fig. 5, we plot the 1, 10, 100, and 1000 $(\Omega\ \mathrm{cm})^{-1}$ electronic conductivity contours as derived from this model. To compare, the conductivity of pure, distilled water at room conditions is 10^{-5} $(\Omega\ \mathrm{cm})^{-1}$, more than six orders of magnitude lower in value than we determine under shock conditions,[42] while the conductivity of iron at room conditions is $\sim 10^5$ $(\Omega\ \mathrm{cm})^{-1}$. The observed reflectivity can thus be attributed to the production of thermally activated electrons, however, not as high in conductivity as standard metals at room conditions. Our observations are consistent with reflectivity observed for laser-driven single-shock experiments on normal (not precompressed) water samples at pressures above 100 GPa, for which temperatures are higher at any given pressure than for the precompressed samples (Fig. 5).[22] This agreement suggests that the model may also be reliable in representing the electronic conductivity of water along the isentrope. If the onset of reflectivity is an indication of an increased electronic contribution to the conductivity, and is both pressure and temperature dependent, our new measurements help to constrain the relative contributions of ionic and electronic conductivities along the icy giant isentrope. From the model, the 10 $(\Omega\ \mathrm{cm})^{-1}\sigma_e$ contour intersects the Neptune isentrope near 125 GPa, while the 100 $(\Omega\ \mathrm{cm})^{-1}\sigma_e$ contour, a

Downloaded 01 Feb 2008 to 128.115.27.10. Redistribution subject to AIP license or copyright; see http://jcp.aip.org/jcp/copyright.jsp

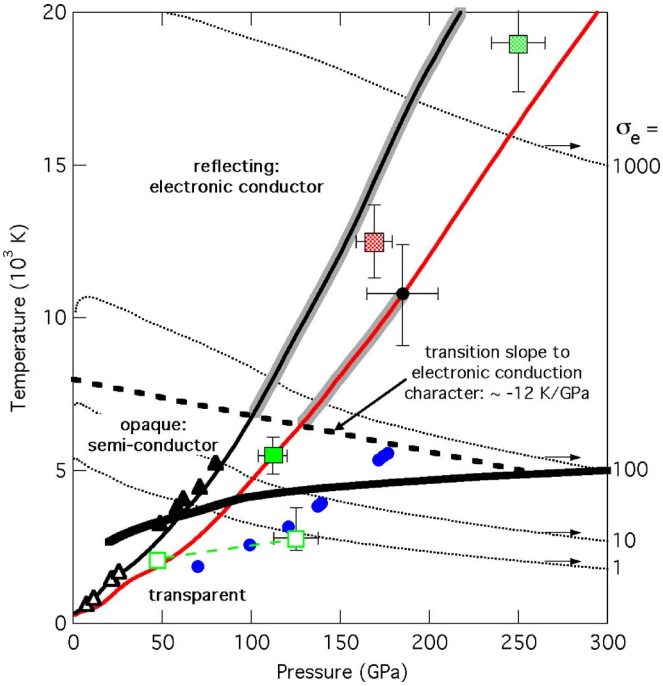

FIG. 5. Pressure vs temperature (T_{SESAME}) phase diagram for shocked precompressed water. Samples that remained transparent at 532 nm (green outlined squares), opaque at 532 nm (green filled square), reflecting at 532 nm (green hatched square), and reflecting at 1064 nm (red hatched square, shaded region along 1 GPa precompression Hugoniot) are plotted with their calculated temperatures. Green dashed line between transparent samples (green outlined squares) shows transparency for the same sample after successive shocks (see description in text and Fig. 3). We interpret opaque water samples as semiconducting, whereas, and reflecting water as due to electronic conduction. The regions are separated by a thick, dashed line with a slope of ~−12 K/GPa. The thick solid curve represents Neptune's isentrope (Ref. 48). The single-shock (precompressed to 1 GPa) Hugoniot of water is plotted as the black (red) curve (Refs. 34 and 35). For reference, we summarize single-shock experiments on water observed to be transparent [open triangles (Ref. 26)], opaque [closed triangles (Ref. 24)], and reflecting [shaded region above ~100 GPa along single-shock Hugoniot (Ref. 22)]. Additionally, the results of shock-reverberation experiments (Ref. 7) are shown [with revised temperature estimates (Ref. 22)] as blue circles. Additionally, we plot the electronic conductivity σ_e as thin, dotted, black lines representing the 1, 10, 100, and 1000 $(\Omega\,\mathrm{cm})^{-1}$ contours.

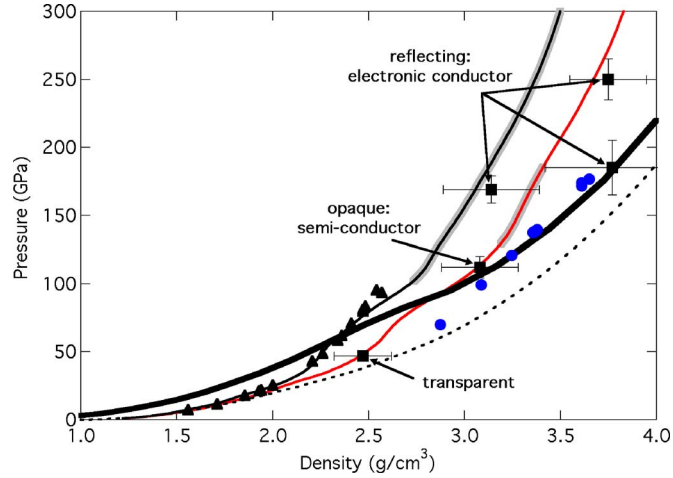

FIG. 6. Density vs pressure phase diagram for shocked precompressed water. This study's measurements are shown as black squares labeled with the optical properties observed: transparent, opaque, or reflecting. Observations of reflecting water along the single-shock (Ref. 22) and 1 GPa precompression Hugoniots are shaded as in Fig. 5. The thick curve represents the isentrope of water centered at 300 GPa (Refs. 34 and 35) along Neptune's isentrope (Ref. 48). The single-shock (precompressed to 1 GPa) Hugoniot of water is plotted as the black (red) curve (Refs. 34 and 35). For reference, early single-shock experiments on water are shown as black triangles (Refs. 6, 24, and 25), and the results of shock-reverberation experiments (Ref. 7) are shown as blue circles. Additionally, the principle isentrope of water is shown as the black, dashed line (Refs. 34 and 35).

conductivity value approaching that of a poor metal, intersects the isentrope near 250 GPa. This suggests that the conductivity in the outer layers is sufficient for dynamo production and involves a combination of electronic and ionic conductions.

Our results compare well with previous observations of the optical properties of water under conditions of high pressure and temperature. Early shock-wave experiments on water along the principal Hugoniot have also documented transparency,[26,40] opacity,[24] and reflectivity.[22] An increase in water's electrical conductivity to ~25 $(\Omega\,\mathrm{cm})^{-1}$ with increasing pressure up to ~30 GPa, followed by constant conductivity to 60 GPa, was inferred to be due to ionic conduction.[6] This conclusion is derived from Raman spectra of single-shocked water up to 26 GPa at a calculated temperature of 1700 K, which remained transparent.[26] The temperatures have been measured in experiments for only the opaque samples (pressures $>\sim 50$ GPa) and are up to 4100 K at 60 GPa (Ref. 24) (Fig. 5).

Recent DAC experiments document transparent water up to 56 GPa and 1500 K, with Raman spectra interpreted as showing evidence of superionicity.[16] For DAC water samples compressed between 6 and 43 GPa and heated to temperatures above ~2000 K, the water was observed to be opaque.[13]

Reverberated-shock experiments to pressures between 70 and 180 GPa show a further increase in conductivity, from 30 to 210 $(\Omega\,\mathrm{cm})^{-1}$, also interpreted as due to ionization of water:[5,7] $H_2O \rightarrow H^+ + OH^-$. Although the temperatures were not measured in these experiments, they are estimated to be ~5400 K at the highest pressures,[22,23] and are likely lower than our own temperatures.

For comparison, the conductivity of shocked metallic hydrogen is ~2000 $(\Omega\,\mathrm{cm})^{-1}$ at 140 GPa and 4400 K,[43] and that of shocked metallic oxygen is ~1000 $(\Omega\,\mathrm{cm})^{-1}$ at 120 GPa and 4500 K (Ref. 44) (the shock temperatures are calculated values in both cases). These conductivities are far higher than the values we infer from our optical measurements, suggesting that if dissociation takes place under shock loading it is not complete over the range of conditions achieved in the present study.

VI. CONCLUSIONS

With five experimental shots, we observe hot, dense water up to ~250 GPa and up to ~19 000 K. Due to the lower temperatures achieved with precompressed samples than in traditional single-shock experiments, we obtain densities that are greater than those measured on the principal Hugoniot (Fig. 6).[6,24–26] We observe three distinct regimes of differing optical properties upon shock compression: transparent, opaque, and reflecting (Table II, Fig. 5).For the experiments at lowest pressures and temperatures, water remains transparent. Our observations cannot verify the previous[6,26] interpre-

Downloaded 01 Feb 2008 to 128.115.27.10. Redistribution subject to AIP license or copyright; see http://jcp.aip.org/jcp/copyright.jsp

tation of high conductivity as due to the ionization of water, but are compatible with this interpretation. Upon transition to the opaque state, water behaves as a semiconductor at temperatures of ~3000–6000 K: the measured conductivity is likely no longer just ionic but also has an electronic contribution and is likely pressure dependent. Above ~6000 K along the precompressed 1 GPa Hugoniot, the concentration of thermally-activated carriers is sufficient to produce metallic-like optical reflectivity with conductivities greater than 100 $(\Omega\ \mathrm{cm})^{-1}$, approaching that of a poor metal (Fig. 5). This has been observed in previous experiments,[22] and is interpreted as the onset of electronic conduction in water caused by the high temperatures reached during shock loading. At pressures and temperatures greater than ~130 GPa and 6600 K, water becomes reflecting at 1064 nm, although it is still opaque at 532 nm. At the most extreme pressure and temperature that we achieved, ~250 GPa and ~19 000 K (T_{SESAME}), we observe water reflecting at visible wavelengths.

Figures 5 and 6 show our measurements compared with the previous investigations of high-pressure and -temperature water. Some of our measurements cluster near Neptune's expected isentrope and suggest that this planet's magnetic field could be sustained by pressure-induced semiconducting (rather than ionic) water at pressures as low as ~100 GPa, more than an order of magnitude lower than the peak pressure achieved in Neptune. Our results thus reinforce the conclusion that water can sustain a magnetic dynamo at fairly shallow levels in the planet, compatible with the strongly quadrupolar nature of the observed magnetic field.[3]

ACKNOWLEDGMENTS

We thank Paul Loubeyre and Agnes Dewaele for extensive experimental and technical help, and R. Chau for help in reanalyzing the results of Ref. 7. We thank the operations staff of the Vulcan Laser Facility at Rutherford Appleton Laboratory for their support. This research was supported by the National Science Foundation and under the auspices of the U.S. Department of Energy by the University of California, Lawrence Livermore National Laboratory under Contract No. W-7405-Eng-48.

[1] W. B. Hubbard, *Planetary Interiors* (Van Nostrand Reinhold, New York, 1984).
[2] D. J. Stevenson, Earth Planet. Sci. Lett. **208**, 1 (2003).
[3] E. C. Stone and E. D. Miner, Science **246**, 1417 (1989).
[4] R. L. Kirk and D. J. Stevenson, Astrophys. J. **316**, 836 (1987).
[5] V. V. Yakushev, V. I. Postnov, V. E. Fortov, and T. I. Yakysheva, J. Exp. Theor. Phys. **90**, 617 (2000).
[6] A. C. Mitchell and W. J. Nellis, J. Chem. Phys. **76**, 6273 (1982).
[7] R. Chau, A. C. Mitchell, R. W. Minich, and W. J. Nellis, J. Chem. Phys. **114**, 1361 (2001).
[8] W. J. Nellis, N. C. Holmes, A. C. Mitchell, D. C. Hamilton, and M. Nicol, J. Chem. Phys. **107**, 9096 (1997).
[9] C. Cavazonni, G. L. Chiarotti, and S. Scandolo, Science **283**, 44 (1999).
[10] S. Stanley and J. Bloxham, Nature (London) **428**, 151 (2004).
[11] A. F. Goncharov and V. V. Struzkhin, Science **273**, 218 (1996).
[12] R. J. Hemley, A. P. Jephcoat, H. K. Mao, C. S. Zha, L. W. Finger, and D. E. Cox, Nature (London) **330**, 737 (1987).
[13] L. R. Benedetti, Ph.D thesis, University of California, Berkeley, 2001.
[14] B. Schwager, L. Chudinovskikh, A. Gavriliuk, and R. Boehler, J. Phys.: Condens. Matter **16**, S1177 (2004).
[15] J.-F. Lin, B. Militzer, V. V. Struzkhin, and E. Gregoryanz, J. Chem. Phys. **121**, 8423 (2004).
[16] A. F. Goncharov, N. Goldman, L. E. Fried, J. C. Crowhurst, I.-F. W. Kuo, C. J. Mundy, and J. M. Zaug, Phys. Rev. Lett. **94**, 125508 (2005).
[17] M. R. Frank, Y. Fei, and J. Hu, Geochim. Cosmochim. Acta **68**, 2781 (2004).
[18] T. Kawamoto, S. Ochiai, and H. Kagi, J. Chem. Phys. **120**, 5867 (2004).
[19] Y. Fei, H. K. Mao, and R. J. Hemley, J. Chem. Phys. **99**, 5369 (1993).
[20] E. N. Avrorin, B. K. Vodolaga, L. P. Volkov, A. S. Vladimirov, V. A. Simonenko, and B. T. Chernovolyuk, JETP Lett. **31**, 727 (1980).
[21] M. A. Podurets, G. V. Simakov, R. F. Trunin, L. V. Popov, and B. N. Moiseev, Sov. Phys. JETP **35**, 375 (1972).
[22] P. M. Celliers, G. W. Collins, D. G. Hicks *et al.*, Phys. Plasmas **11**, L41 (2004).
[23] In the course of analyzing our data and previous results, we discovered that the temperatures listed in Table I of Ref. 7 are incorrect. We recalculated the conditions of Ref. 7 two ways. First, by computing the first shock state transmitted from the first anvil, followed by the reflected shock state at the second anvil and then following the isentrope to the final pressure. Second, we simulated the reverberation impact with a Lagrangian hydrocode (which follows the entire multiple shock sequence), and found that most of the entropy is deposited in the first two shocks. Both calculations employed the SESAME 7150 equation of state for water (Ref. 34), which is known to agree with the temperature measurements along the Hugoniot by Lyzenga *et al.* (Ref. 24), and the SESAME 7410 or 7411 EOS (Ref. 35) tables for the sapphire anvils. The estimated temperatures calculated with both methods and using either of the sapphire EOS tables agreed to better than 2% for all cases in Ref. 7.
[24] G. A. Lyzenga, T. J. Ahrens, W. J. Nellis, and A. C. Mitchell, J. Chem. Phys. **76**, 6282 (1982).
[25] L. P. Volkov, N. P. Voloshin, R. A. Mangasarov, V. A. Simonenko, G. V. Sin'ko, and V. L. Sorokin, JETP Lett. **31**, 513 (1980).
[26] N. C. Holmes, W. J. Nellis, and W. B. Graham, Phys. Rev. Lett. **55**, 2433 (1985).
[27] K. K. M. Lee, L. R. Benedetti, A. Mackinnon, D. G. Hicks, S. J. Moon, P. Loubeyre, F. Occelli, A. Dewaele, G. W. Collins, and R. Jeanloz, AIP Conf. Proc. **620**, 1363 2002.
[28] P. Loubeyre, P. M. Celliers, D. G. Hicks *et al.*, High Press. Res. **24**, 25 (2004).
[29] Y. B. Zeldovich and Y. P. Raizer, *Physics of Shock Waves and High Temperature Phenomena* (Academic, New York, 1967).
[30] I. N. Ross, M. S. White, J. E. Boon, D. Craddock, A. R. Damerell, R. J. Day, A. F. Gibson, P. Gottfeldt, D. J. Nicholas, and C. J. Reason, IEEE J. Quantum Electron. **QE-17**, 1653 (1981).
[31] L. M. Barker and R. E. Hollenbach, J. Appl. Phys. **43**, 4669 (1972).
[32] P. M. Celliers, G. W. Collins, L. B. DaSilva, D. M. Gold, and R. Cauble, Appl. Phys. Lett. **73**, 1320 (1998).
[33] P. M. Celliers, D. K. Bradley, G. W. Collins, D. G. Hicks, T. R. Boehly, and W. J. Armstrong, Rev. Sci. Instrum. **75**, 4916 (2004).
[34] F. H. Ree, J. Chem. Phys. **76**, 6287 (1982)
[35] S. P. Lyon and J. D. Johnson, Los Alamos National Laboratory Report No. LA-UR-92-3407, 1992 (unpublished)..
[36] A. V. Bessarab, N. V. Zhidkov, S. B. Kormer, D. V. Pavlov, and A. I. Funtikov, Sov. J. Quantum Electron. **8**, 188 (1978).
[37] *Experimental Data on Shock Compression and Adiabatic Expansion of Condensed Matter*, edited by R. F. Trunin (RFNC-VNIIEF, Sarov, 2001).
[38] M. Takeda, H. Ina, and S. Kobayashi, J. Opt. Soc. Am. **72**, 156 (1982).
[39] L. M. Barker and K. W. Schuler, J. Appl. Phys. **45**, 3692 (1974).
[40] Y. B. Zeldovich, Sov. Phys. Dokl. **6**, 494 (1961).
[41] A. Dewaele, J. Eggert, P. Loubeyre, and R. LeToullec, Phys. Rev. B **67**, 094112 (2003).
[42] A. A. Brish, M. S. Tarasov, and V. A. Tsukerman, Sov. Phys. JETP **11**, 15 (1960).
[43] S. T. Weir, A. C. Mitchell, and W. J. Nellis, Phys. Rev. Lett. **76**, 1860 (1996).
[44] M. Bastea, A. C. Mitchell, and W. J. Nellis, Phys. Rev. Lett. **86**, 3108 (2001).
[45] H. K. Mao, P. M. Bell, J. W. Shaner, and D. J. Steinberg, J. Appl. Phys. **49**, 3276 (1978).
[46] A. Saul and W. Wagner, J. Phys. Chem. Ref. Data **18**, 1537 (1989).
[47] H. Shimizu, T. Nabetani, T. Nishiba, and S. Sasaki, Phys. Rev. B **53**, 6107 (1996).
[48] W. B. Hubbard, M. Podolak, and D. J. Stevenson, in *Neptune and Trition*, edited by D. P. Cruikshank (University of Arizona Press, Tucson, AZ, 1995), p. 109.

Downloaded 01 Feb 2008 to 128.115.27.10. Redistribution subject to AIP license or copyright; see http://jcp.aip.org/jcp/copyright.jsp